HHS Public Access

Author manuscript

Acta Biomater. Author manuscript; available in PMC 2020 August 24.

Published in final edited form as:

Acta Biomater. 2019 August ; 94: 160–172. doi:10.1016/j.actbio.2019.02.054.

Microporous annealed particle hydrogel stiffness, void space size, and adhesion properties impact cell proliferation, cell spreading, and gene transfer

Norman F. Truong[1], **Evan Kurt**[3], **Nairi Tahmizyan**[1], **Sasha Cai Lesher-Pérez**[1], **Mabel Chen**[1], **Nicole J. Darling**[1], **Weixian Xi**[1,2], **Tatiana Segura**[1,4]

[1]Department of Chemical and Biomolecular Engineering, University of California Los Angeles, Los Angeles, CA

[2]Department of Orthopaedic Surgery, University of California Los Angeles, Los Angeles, CA

[3]Department of Biomedical Engineering, Duke University, Durham, NC

[4]Current affiliations: Departments of Biomedical Engineering, Neurology, and Dermatology, Duke University, Durham, NC

Abstract

Designing scaffolds for polyplex-mediated therapeutic gene delivery has a number of applications in regenerative medicine, such as for tissue repair after wounding or disease. Microporous annealed particle (MAP) hydrogels are an emerging class of porous biomaterials, formed by annealing microgel particles to one another *in situ* to form a porous bulk scaffold. MAP gels have previously been shown to support and enhance proliferative and regenerative behaviors both *in vitro* and *in vivo*. Therefore, coupling gene delivery with MAP hydrogels presents a promising approach for therapy development. To optimize MAP hydrogels for gene delivery, we studied the effects of particle size and stiffness as well as adhesion potential on cell surface area and proliferation and then correlated this information with the ability of cells to become transfected while seeded in these scaffolds. We find that the void space size as well as the presentation of integrin ligands influence transfection efficiency. This work demonstrates the importance of considering MAP material properties for guiding cell spreading, proliferation, and gene transfer.

Abstract

Microporous annealed particle (MAP) hydrogels are an emerging class of porous biomaterials, formed by annealing spherical microgels together *in situ*, creating a porous scaffold from voids between the packed beads. Here we investigated the effects of MAP physical and adhesion properties on cell spreading, proliferation, and gene transfer in fibroblasts. Particle size and void space influenced spreading and proliferation, with larger particles improving transfection. MAP stiffness was also important, with stiffer scaffolds increasing proliferation, spreading, and transfection, contrasting studies in nonporous hydrogels that showed an inverse response. Last,

RGD ligand concentration and presentation modulated spreading similar to non-MAP hydrogels. These findings reveal relationships between MAP properties and cell processes, suggesting how MAP can be tuned to improve future design approaches.

Keywords

gene delivery; non-viral; MAP hydrogel; porous; polyplex

1 Introduction

Non-viral gene delivery has been an invaluable tool used not only to study biological processes such as differentiation, but also serve as an alternative to viral gene therapy, particularly in tissue regeneration applications. However, the broader applicability of non-viral gene delivery is limited by overall low transfection efficiency. Thus, strategies to increase the efficiency of non-viral gene delivery are critical to improving biological studies both *in vitro* and *in vivo*. While there has been considerable research done on improving gene carriers[1,2] and vector DNA constructs[3], many studies have also explored the role the cellular microenvironment on key cellular processes which influence gene transfer. Such features of the microenvironment include substrate chemistry and charge[4], extracellular matrix protein composition[5,6], cell adhesion ligand presentation and concentration[7,8], substrate stiffness[8,9], and surface topography[10]. Importantly, these key features triggered different responses when cells were seeded in two dimensions compared to in three dimensions. Culturing cells in three dimensions (3-D) in hydrogel scaffolds is crucial for biomedical applications, as it better mimics the native tissue environment, serving as a more accurate *in vitro* model to study biological processes or to test new therapies[11]. The viscoelastic properties of hydrogels must be tailored for the particular tissue of interest, with stiffer systems for applications in skin[12], or softer ones as in the brain[13,14]. The locally observed cellular microenvionment is especially relevant to the development of new hydrogel biomaterials used to locally deliver therapeutic genes to infiltrating cells for regenerative medicine applications such as in wound healing, stroke recovery, or cartilage and bone regeneration.

One class of biomaterials recently developed by our laboratory for such tissue regeneration applications is the microporous annealed particle (MAP) hydrogel, which consists of microscale modular hydrogel-based building blocks that anneal to one another *in situ* upon injection to form a porous scaffold[15,16]. The microscale pores allow for homogeneous distribution of incorporated cells for culture *in vitro*. The MAP scaffold also promotes cell proliferation and infiltration throughout the scaffold differently from culture in nonporous hydrogels *in vivo*, as rates of cell spreading and infiltration are no longer dependent on the local cell-mediated degradation of the hydrogel. In addition, the MAP scaffold shows significant promise in promoting tissue regeneration in large part due to its inherent porous structure and the ability to seamlessly fill the wound cavity due to its injectability. In a murine cutaneous wound healing model, MAP scaffold injections accelerated tissue formation and vascularization[15]. Similarly, in a murine stroke model, the MAP scaffold reduced inflammation, increased peri-infarct vascularization, and induced migration of

neuroprogenitor cells into the stroke site[17]. In both cases, the MAP scaffolds were able to have stiffness and resulting void space adjusted for compatibility in the target tissues. Quantification of native tissue porosity is challenging from literature, with studies developing complex models to account for voids[18,19]. The MAP system allows for emulating the native tissue stiffness while optimizing the void space as a function of microgel size, rather than mimic the intricacies of tissues, to maximize cell infiltration and spreading. Coupling such a material with the therapeutic potential of non-viral gene delivery may yield positive outcomes for therapy development. Previously, MAP scaffolds were shown to modulate cell response from transfection differently than standard nonporous hydrogels, with altered cell spreading and proliferation mechanisms, in addition to polyplex uptake and transgene expression pathways[20].

Here, we investigated the effects of several different physical and cell adhesion properties of MAP hydrogels on non-viral gene delivery. Specifically, we explored how MAP scaffold properties such as modular block size, stiffness, cell adhesion ligand concentration and presentation, and integrin specificity can modulate cell spreading, proliferation, and non-viral gene transfer to cells cultured within the scaffold.

2 Methods

2.1 Preparation of hyaluronic acid-norbornene (HA-Norb)

To modify hyaluronic acid (HA) to contain norbornene functional groups, 1 g of 60 kDa sodium hyaluronan (Genzyme, Cambridge, MA) and 3.111 g 4-(4,6-dimethoxy-1,3,5-triazin-2-yl)-4-methyl-morpholinium chloride (DMTMM) (Thermo Fisher Scientific, Waltham, MA) were each dissolved in 40 mL 200 mM MES buffer pH 5.5 (molar ratio of ~1:633 for HA to DMTMM). The two solutions were combined and stirred for 10 minutes to allow for activation of the carboxylic acid (Figure 1A). 0.677 mL 5-norbornene-2-methylamine (TCI America, Portland, OR) was added dropwise to the reaction mixture (molar ratio of ~1:343 for activated HA to NMA), which was then allowed to react overnight at 25°C with constant stirring. The reaction product was then precipitated in ethanol, filtered to collect the solid, dissolved in 2 M NaCl in water, and dialyzed under running deionized water for 24 hours. The final product was then filtered, flashfrozen, and lyophilized. The extent of modification was confirmed via ^{1}H-NMR spectrometry. ^{1}H-NMR shifts of attached norbornene groups in the product in D_2O are δ = 6.33 and 6.02 (vinyl protons, endo), and 6.26 and 6.23 ppm (vinyl protons, exo). The integrations of these peaks were normalized to the peak corresponding to the methyl group on the HA monomer at δ = 2.0 ppm to determine percent of HA monomers modified to contain norbornene groups. Following synthesis, the HA precursor and HA-Norb product were assessed with electrophoretic light scattering (ELS) on a Malvern ZetaSizer ZS instrument to determine if the polymers are prone to self-assembly. Size and electrophoretic mobility were assessed in triplicate using the default run parameters, at up to 150 scans, for stabilized measurements to derive the zeta potential.

2.2 Synthesis of polyethylene glycol-tetrazine (PEG-tet)

PEG-tet was synthesized by combining 100 mg 4-arm 20kDa PEG-thiol (NOF America, White Plains, NY) and 15 mg methyltetrazine-PEG_4-maleimide (Kerafast, Boston, MA) for a Mal/SH ratio of 1.05 (or molar ratio of 1:5.8 for PEG-thiol to Tet-Mal), each dissolved in 0.5 mL dichloromethane (DCM). 1 μL of trimethylamine was added (0.5 molar equivalent) and the mixture was allowed to stir at 25°C for 4 hours while protected from light (Figure 1B). The reaction product was precipitated in 50 mL of cold diethyl ether and allowed to dry under vacuum overnight. Modification of the thiol groups with the tetrazine was verified through ^{1}H-NMR, observing shifts of attached tetrazine groups in the product in D_2O at δ = 7.24 and 8.52 (phenyl protons, at ester and tetrazine ends respectively). The integrations of these peaks were normalized to the large 4-arm PEG peak at δ = 3.25 ppm and compared to determine percent modification with the tetrazine groups.

2.3 HA microgel formation and purification

HA-Norb microgels were prepared using a batch water-in-hexane emulsion technique. 1 mL of gel precursor solution was prepared in HEPES buffer pH 8.3 with HA-Norb at a final concentration of 3.5 wt%, lithium phenyl(2,4,6-trimethylbenzoyl)phosphinate photo-initiator (LAP; TCI America) at 2.2 mM, thiolated RGD peptide (RGDSPGERCG; Genscript, Piscataway, NJ) at 100, 250, 500, or 1000 μM, and tris(2-carboxyethyl)phosphine (TCEP) at 25% of the total thiol molarity (i.e. mmol TCEP:mmol thiols = 1:4). Once all the components were mixed, a 50 mM stock of dithiothreitol (DTT) (Thermo Fisher Scientific) was added as the crosslinker to achieve a crosslinking ratio (mmol SH/mmol HA) of 14, 28, or 56. For RGD clustering, a portion of the HA-Norb was combined with the total amount of RGD peptide and pre-reacted by exposing the solution to UV light for 1 minute at 10 mW/cm^2 in the presence of the appropriate amount of LAP and TCEP, after which the remaining HA-Norb, LAP, and TCEP were added, along with DTT. To generate microgels containing different fibronectin fragments without clustering, the recombinant fragments, provided to us by Dr. Thomas Barker of the University of Virginia, were combined in lieu of RGD along with the other gel components as described above to a final concentration of 5 μM. This final gel precursor solution was then pipetted into a round-bottom flask containing 10 mL 3% span-80 in hexane continuously stirring at 800 rpm, then mixed by pipetting up and down 9 times to generate a stable emulsion. The flask's contents were then purged with argon and exposed to UV light at 15 mW/cm^2 for 10 minutes to trigger the norbornene-thiol crosslinking reaction to form microgels.

Next, the crosslinked microgels in hexane was transferred into a conical tube and centrifuged at 1000 x g and washed with hexane three times. The microgels were then transferred to 1% Pluronic F107 in PBS for 30 min to allow for swelling before sieving using 200 μm, 100 μm, 60 μm, and 20 μm (PluriSelect, Leipzig, Germany) pore size strainers. During sieving, microgels were washed with 10 mL 1% Pluronic in PBS and 50 mL PBS. The collected microgels were then autoclaved and pelleted by centrifugation at 14000 x g for 5 minutes, after which the supernatant was removed and microgels were stored at 4°C until further use.

2.4 Alexa Fluor 647 tetrazine synthesis and labelling of microgels

To synthesize Alexa Fluor 647 tetrazine, 2.8 mg PEG dithiol (MW 3500 Da) (JenKem Technology USA, Plano, TX) and 0.41 mg methyltetrazine-PEG4-maleimide (Kerafast) were each dissolved in 1 mL dichloromethane and combined in a glass vial. 0.11 μL triethylamine (SigmaAldrich) and 1 mg Alexa Fluor-647 maleimide (Thermo Fisher Scientific) were then added and the reaction was allowed to proceed overnight at 25°C protected from light. The reaction was then precipitated in 10 mL cold diethyl ether, centrifuged at 14000 x g for 5 minutes to pellet the precipitate, and the diethyl ether was decanted. The residual diethyl ether was removed under vacuum overnight. The resulting product was dissolved at 1 mg/mL in dimethylformamide and stored at −20°C.

To fluorescently tag 200 μL microgels, Alexa Fluor 647 tetrazine was diluted in 100 μL PBS to a concentration of 0.015 mM and combined with the microgels. The mixture was then incubated at 37°C for 1 hour with agitation. Microgels were washed three times by filling tube with PBS, centrifuging at 14000 x g for 5 minutes to pellet beads, and aspirating liquid.

2.5 Microgel size distribution

After sieving and tagging with fluorophore, free microgels in PBS were imaged as z-stacks using confocal microscopy using a 10x objective to obtain a maximum intensity projection. These images were then analyzed using the particle analysis toolkit in ImageJ to obtain diameter measurements of 400 to 1700 microgels for each condition, which were subsequently plotted using the Seaborn visualization package in Python.

2.6 Microgel annealing to generate MAP scaffolds

A 5.32 mM solution of PEG-Tet in PBS was mixed with microgels at a 1:6 volumetric ratio of PEG-Tet to microgels and immediately centrifuged at 14000 x g for 3 minutes. Excess liquid was removed, and 15 μL of gel was pipetted into each well and allowed to anneal for 1 hour at 37°C.

2.7 Preparation of cell culturing devices

A custom negative mold was printed using a 3D, Form 2 stereolithography printer (Formlabs, Inc.). Cell culture devices were cast using soft lithography to produce a PDMS reservoir for cell culture. The culture wells were composed of a cylindrical culture section (3 mm in diameter and 5 mm tall), enabling a maximum of 35 μL of volume. Additionally, a conical media reservoir above the cylindrical culturing section was able to contain up to 150 μL of media. Specific dimensions of the mold, and subsequently the PDMS wells, can be found in Supplementary Figure 1. To fabricate PDMS culturing devices, 70 g of Sylgard 184 PDMS (Dow Corning) was preparing according to the manufacturer's instructions and poured into a 10 cm x 10 cm square dish. The mold was placed in the PDMS, and the PDMS was degassed by applying a vacuum for 1 hour. Subsequently, the PDMS was allowed to cure at 60°C for 4 hours in a convection oven. The PDMS slab was then cut into three-well pieces and plasma-bonded to cover glass slides using a corona plasma gun. PDMS triplicate well-slides were then autoclaved prior to use for cell culture and experimental evaluation.

2.8 Cell culture and seeding HDFs in MAP scaffolds

Human dermal fibroblasts (HDF; Cell Applications, Inc., San Diego, CA) were maintained in culture in Dulbecco's modified Eagle's medium (Thermo Fisher Scientific) containing 10% fetal bovine serum (Thermo Fisher Scientific) at 37°C and 5% CO_2. Media was changed every 2–3 days.

To seed cells in MAP scaffolds, 100 μL microgels were first equilibrated in supplemented media for 30 minutes before pelleting and removing supernatant. HDFs were trypsinized and 1.2×10^5 cells were pelleted by centrifugation at 250 x g for 5 minutes. Media supernatant was aspirated and equilibrated microgels in PEG-Tet solution (as described in section 2.6) were then added to the cell pellet and mixed thoroughly by pipetting. Importantly, prior to gel/cell seeding, 6 μL of sterile 1% agarose in PBS was added to the wells to coat the glass surface and allowed to cool to 25°C to prevent cell attachment to glass. 15 μL of gel plus cells was then pipetted into each well in the PDMS culturing device. The MAP gel was allowed to anneal for 1 hour at 37°C. After annealing, the wells were filled with 150 μL supplemented media containing 50 μg/mL primocin (InvivoGen, San Diego, CA).

2.9 Void space analysis

Annealed MAP scaffolds of various microgel bead sizes were incubated with PBS containing 1 μg/mL 500 kDa tetramethylrhodamine isothiocyanate-dextran (TRITC-dextran) (Sigma-Aldrich, St. Louis, MO) to fill the void space in between microgels, as it is too large to penetrate the microgel's polymer network. The labelled void space was imaged using confocal microscopy to obtain 200-μm z-stacks. The z-stacks were imported into IMARIS to generate surface renders, and void space volumes were quantified as a fraction of the total volume represented by the z-stack. A minimum of 4 measurements were made for each MAP scaffold.

2.10 Oscillation rheometry

Stiffness of both nonporous HA-Norb hydrogels and of annealed MAP gels were measured as the storage modulus (G') using a plate-to-plate rheometer (Physica MCR, Anton Paar, Ashland, VA). To create a nonporous HA-Norb gel, 45 μL of the gel precursor solution was prepared as described in section 2.3 and pipetted onto a Sigmacote-treated (Sigma-Aldrich) glass slide. 1mm-thick spacers were placed on either side of the slide and a second Sigmacote-treated slide was placed on top to sandwich the gel precursor solution and fastened into place using binder clips. The gel was exposed to UV light at 15 mW/cm^2 for 1 minute, then flipped and exposed for another minute for uniform crosslinking. The crosslinked gel was transferred into PBS and allowed to swell overnight. A frequency sweep was performed on the hydrogels using a strain of 0.2% with an angular frequency range of 0.5 to 10 rad/s. To measure the storage modulus of an annealed MAP gel, 50 μL microgels with PEG-Tet were pipetted directly onto the rheometer stage. The measuring position was set to 1mm and the gel was allowed to incubate with humidity for 1 hour to allow for annealing. Once the gel was annealed, a frequency sweep was performed on the hydrogels using a strain of 1% with an angular frequency range of 0.5 to 10 rad/s.

2.11 Cell staining, imaging, and quantification of cell spreading

MAP gels with cells cultured for 2 days were fixed in 1% paraformaldehyde for 15 minutes at 25°C. The cultures were permeabilized in 0.1% Triton X-100 in PBS and stained using DAPI (Sigma-Aldrich) for cell nuclei and rhodamine phalloidin (Thermo Fisher) for cell actin per manufacturer's guidelines for 1 hour. Gels were washed with PBS before z-stack imaging with a Nikon confocal. To quantify cell spreading, the z-stacks were imported into IMARIS to generate surface renders of cell actin for surface area quantification and to count nuclei.

2.12 Transfection of MAP gel culture and assay for transgene expression

Transfection was performed two days after seeding cells in MAP gels to allow for adequate spreading. DNA polyplexes were prepared by complexing plasmid DNA encoding for Gaussia luciferase (GLuc) with jetPEI (Polyplus-Transfection, Illkirch, France) according to manufacturer's instructions. Briefly, 0.25 μg DNA was diluted in 10 μL of 150 mM NaCl and 0.5 μL jetPEI was diluted in a separate tube in 10 μL of 150 mM NaCl, for an N/P of 5 based on the manufacturer protocol. Similar formulations were prepared for 0.125 ug and 0.5 ug doses of the plasmid DNA for the same N/P ratio. The jetPEI solution was then added to the DNA solution, immediately vortexed, and allowed to incubate for 15 min at 25°C to allow for complexation. Amounts were scaled up depending on DNA dose and number of wells, but the polyplex volume administered to each well remained constant (20 μL of polyplexes were added to each well as a bolus administration). After 4 hours of polyplex exposure, the polyplex-containing media was removed and replenished with fresh media.

To verify that cells throughout the scaffold were uniformly transfected in the z-direction, plasmid DNA was mixed with the fluorescent dye, YOYO-1 (Thermo Fisher Scientific), at a ratio of 1:50 YOYO-1:base-pair DNA and was allowed to incubate for 30 minutes at 25°C. YOYO-1-labeled DNA was then used to prepare polyplexes as mentioned above. MAP gels containing cells and YOYO-1 polyplexes were then imaged using confocal microscopy to obtain z-stacks, and percent co-localization of YOYO-1 polyplexes with cell actin was quantified for each image in the z-stack to confirm consistent transfection in the z-direction.

Transfection was quantified by measuring expression of GLuc using the BioLux Gaussia Luciferase assay kit (New England Biolabs, Ipswich, MA) per manufacturer's protocol. Conditioned media was collected from each well at each time point. Briefly, 20 μL of each sample was mixed with 50 μL of substrate solution, pipetted for 2 to 3 seconds to mix, and read for luminescence with a 5 second integration time using a Modulus Fluorometer (Turner BioSystems, South San Francisco, CA).

2.13 Cell viability

Cell viability was quantified using the PrestoBlue assay (Thermo Fisher Scientific) per manufacturer's instructions. At specified times, the media in each well was replaced with a solution of 10 μL of the PrestoBlue reagent mixed with 90 μL of media. After 3 hours, 90 μL from each well were transferred into a 96-well plate and fluorescence was read using a BioTek plate reader at an excitation wavelength of 560 nm and an emission wavelength of 590 nm.

2.14 Statistical analysis

Statistical analysis and plotting were performed using Prism 6. Experiments were repeated two times with three independent gel samples in each experiment. Statistics assumed that gel samples, which were cast independently, were statistically independent from each other. Statistical significance was assessed using a 95% confidence interval using a one-way ANOVA with Tukey post-hoc test, unless otherwise noted. All error is reported as the standard deviation of error (SD).

3 Results and discussion

3.1 Analysis of gel physical properties

To synthesize microgels, HA-Norb was first prepared using amine-carboxylic acid chemistry utilizing the carboxylic acid in the backbone of HA (one per monomer) and a free amine-containing norbornene molecule (Figure 1A). NMR analysis of the modified polymer revealed that 41.85% of the HA monomers were reacted to contain the norbornene functional group, based on the available carboxylic acids per repeating HA monomer. HA microgels were produced using a water-in-hexane emulsion and UV light to trigger a thiolene reaction between the norbornene groups on the HA backbone and the thiols of the DTT crosslinker. The resulting microgels were polydisperse with diameters ranging from 10 to greater than 200 μm, but are all spherical in shape. To ensure that size distributions were not a result of self-assembly by the HA-Norb material prior to crosslinking, due to possible interactions from the hydrophobic norbornene groups, ELS was used to determine the zeta potential of the material. Neither the precursor stock HA (at −27.4 ± 0.4 mV) nor the final HA-Norb product (at −28.3 ± 2.4 mV) showed significant electrostatic interactions to suggest that aggregation occurs. To narrow down the size range, microgels were purified to remove hexane and surfactant and swelled in PBS before sieving through pore size ranges of 20–60 μm, 60–100 μm, and 100–200 μm to generate microgel populations of different sizes and of reduced polydispersity. A size distribution of each size range was obtained via analysis of confocal microscopy images (Figure 2A–B). The average diameters and standard deviations of these populations were 54.25 ± 29.11 μm, 86.04 ± 20.25 μm, and 150.76 ± 44.14 μm, respectively. Microgels with diameters outside the nominal sieving boundaries were also binned, which may be due to the ability of the viscoelastic microgels to squeeze through sieve pores. However, further studies are necessary to determine if this is the case, given that microgel crosslinking and stiffness are varied based on the target application.

MAP scaffolds were generated by annealing microgels within a culture well using a click reaction of the norbornene groups at the surfaces of the beads and a separate 4-arm PEG-tetrazine (PEG-Tet) crosslinker. Briefly, the crosslinker was prepared as described using a 4-arm PEG-thiol and Methyl-tetrazine-PEG4-Maleimide. NMR analysis of the modified polymer revealed that a 98% of the free thiols were converted to the maleimide-linked tetrazine groups. Concentrated fluorescently tagged microgels were mixed with PEG-Tet crosslinker and allowed to anneal to generate MAP scaffolds within custom PDMS culture devices (Figure 2C). To enable visualization and quantification of the void space between each scaffold, a high-molecular-weight fluorescent TRITC-dextran solution, which does not penetrate the microgels, was added to fill the void space within the annealed gel. Z-stack

images were taken to obtain images of the void space between the microspheres (Figure 2D). Use of IMARIS to detect and render surfaces of these void spaces in three dimensions subsequently allowed us to measure void space fractions of these scaffolds (Figure 2E–F). No significant differences in void fraction between gels of different microgel diameters were observed, with void fractions ranging from 0.22 to 0.25. While the close random packing void fraction of a stiff monodisperse bead population is reported to be ~0.36, this value has been demonstrated to decrease with increasing polydispersity of the bead population, such as the ones observed in this study (polydispersity index 0.537, 0.235, and 0.293 for the small, medium, and large microgel populations, respectively)[21]. Furthermore, the viscoelastic nature of the microgels may allow them to pack more densely than an identically distributed population of stiff beads, although individual bead rheology would be required to derive the Young's modulus. We speculate that packing density may increase with decreasing stiffness of microgels. In a previous study, Sideris et al.[16] calculated the void fraction of MAP scaffolds formed with microfluidicsgenerated microgels as 11–15%. This discrepancy with our results may be due to two factors. First, this earlier study computed void fraction by analyzing two-dimensional images individually instead of performing analysis on a three-dimensional render. Second, the inherent mechanical properties of the microgels used in this study were different, due to the different crosslinking chemistry and ratio of crosslinker used to form the microgels. We note that the microfluidic setup was able to produce a more monodispersed range of bead sizes, but the production time is much longer due to slow flow rates to accommodate a different bead crosslinking chemistry, and the end result is the same as the faster batch production used here when followed by rounds of sieving for bead size ranges. Another important factor is the microgel morphology, with no difference in shape present in the annealed microgels, as seen in the 3D renderings of the z-stack. While the solution is heterogeneous from the varied bead sized produced using the batch production method, despite filtering afterwards, packing itself does not appear to induce changes to the bead shape. It is speculated that as there is no physical pressure applied on the scaffold that could warp bead shape, the microgels retain their spherical morphology since the annealed scaffold acts as a hydrogel in media solution. This is the same regardless of how the beads are created, batch or microfluidic, since the spherical geometry and annealing concept is the same. These factors are important to consider when selecting a method to produce MAP for 3-D culture.

We next characterized the rheological properties of the MAP scaffolds used in this study. Three crosslinking ratios of 14, 28, and 56 mmol SH:mmol HA were used to generate microgels to be used for annealing. Oscillation rheometry was performed on both the nonporous gel formulation as well as the annealed MAP scaffold. The storage modulus (G') measurement of the nonporous gel formulation is representative of the local microgel stiffness experienced by a cell which is adhered to a microgel, while the storage modulus of the annealed MAP scaffold provides an overall characterization of the bulk rheological properties of the scaffold as a whole. Taken together, these two measurements provide a more comprehensive characterization which is relevant to cell mechanosensing of the microenvironment. As expected, gels were stiffer with higher concentrations of crosslinker (Figure 2G–H). Previous studies have also shown the relation with increased crosslinking

resulting in increased G' and G", but as stated earlier, further analysis on individual beads could give insight into how packing varies based on the degree of crosslinking.

3.2 Cell culture and transfection in MAP gel

Before evaluating which factors govern transfection and spreading for cells cultured inside MAP scaffolds, we first wanted to ensure that seeded cells could be uniformly transfected after cell spreading had occurred within MAP pores. From the benefits of using MAP for wound regeneration, with past studies in mouse models[15], human dermal fibroblasts (HDF) were used for the 3-D culture. HA microgels were mixed with HDFs and subsequently annealed to form a cell-seeded scaffold (Figure 3A). To confirm cells throughout the scaffold were able to be transfected with a bolus polyplex administration, cells and polyplexes in the scaffold were simultaneously visualized by transfection with polyplexes labeled with YOYO-1, a nucleic acid dye, and subsequently fixing and staining cell actin with phalloidin (Figure 3B). Cell morphology and polyplex uptake were monitored over the first 24 hours of transfection. Percent co-localization of YOYO-1-tagged polyplexes with the labeled cytoskeletal actin was relatively consistent throughout the scaffold, confirming that cells were seeded homogenously throughout the scaffold, especially in the z-direction, and that they were able to be uniformly transfected (Figure 3C–D). However, it is noted that due to the nature of the cell culture devices, image resolution was lost at higher z-stacks, hence the representative image only showing a lower 1 mm slice of the overall gel. Previous studies have confirmed that cells are distributed evenly throughout the annealed gels[15,16], with cells rapidly spreading within the first few hours of 3-D culture following annealing and that no precipitation through the voids observed, so it was assumed to hold true for the polyplexes as well in higher z-stacks.

To measure and compare levels of transfection between conditions, plasmid DNA encoding for the secreted marker protein Gaussia luciferase (GLuc) was complexed with jetPEI, an efficient commercially available polyethyleneimine (PEI)-derived cationic polymer, to form polyplexes. Levels of GLuc expression were easily tunable by controlling the amount of DNA polyplexes used during transfection, with more DNA achieving higher transgene expression (Figure 3E). However, administering high doses of DNA polyplexes initially had an adverse effect on cell viability, although viability was largely restored by day 6 (Figure 3F). The toxicity at higher doses was expected from previous studies with HDF cells, with only 0.25 ug being the optimal dose to balance transgene expression and cell viability. This amount was used for all subsequent experiments with the HDFs. It is important to note that while PrestoBlue correlates cell metabolic activity to viability over the days to monitor, it is possible that the trends could be due to other mechanisms aside from cell death, such as adapting to the scaffold. Previous studies have shown that the MAP scaffold itself does not impact cell viability negatively[15], with the norbornene-tetrazine click reaction releasing only N_2 gas[24,25] that escapes through the MAP voids, and that the trends are similar to those observed when transfecting in 2-D[20]. In addition, no difference in cell morphology was observed between the different polyplex concentrations. Cell viability could be improved through the use of less toxic cationic polymers to complex with DNA, although a vehicle comparison was not within the scope of this study.

3.3 Effects of MAP physical properties on transfection

We next sought to understand how the physical properties of MAP hydrogels, specifically microgel bead size and stiffness, can be controlled to modulate cell spreading, proliferation, and transgene expression. Multiple studies have previously investigated the role of scaffold microarchitecture, namely pore size, on cell morphology and proliferation, albeit with different conclusions on the nature of the relationship depending on cell type, void fraction, and pore shape[26–30]. For example, HDFs seeded in silk fibroin scaffolds 200–250 μm diameter pores exhibited more proliferation than those seeded in scaffolds of smaller pore sizes[29]. In addition, pore shape and topography may also affect cell spreading and migration, as converging or diverging orientations of paths ahead of migrating cells in a matrix have been demonstrated to result in different patterns of cell cytoskeleton polarization and migration[31]. Here we tested the effects of changing microgel size to control scaffold architecture, which would not only increase or decrease pore size while maintaining a constant overall porosity (Figure 2F) but would also modify the topographical curvature of the pore surfaces. Other methods of modifying the architecture include changing the shape of the microgels, which would also affect tortuosity and substrate curvature, although this was not evaluated here.

To investigate microgel size, the three microgel distributions as described in Figure 2A–B were used, while the other gel formulation parameters were kept constant at a crosslinking ratio (SH/HA) of 14, RGD concentration of 500 μM, and RGD clustering ratio of 2:1 mmol RGD:mmol HA. Seeding HDFs in gels of the smallest bead size (20–60 μm sieving range) resulted in less spreading, lower levels of proliferation, and decreased transgene expression than in gels of either of the two larger bead size ranges (60–100 μm and 100–200 μm sieving range) (Figure 4). The relatively low spreading and proliferation in MAP scaffolds made using the smallest microgel size may be due to the smaller pore size of these scaffolds, which can limit the extent of cell spreading. This finding may be extended to the MAP scaffold architecture, in which changing substrate curvature as determined by microgel and diameter may potentially modulate cell morphology, migration, proliferation, and subsequently transfection.

The effects of substrate stiffness on various cellular processes have been well-documented. In general, adhesion, spreading, and proliferation of fibroblasts and other adherent cell lines increase with increasing substrate stiffness for cells cultured in 2-D[32,33]. The range of microgel stiffnesses tested in this study (nonporous G’ 1810 – 3646 Pa) corresponds with a subset of stiffnesses which was previously shown to result in a highly differential spreading response in mouse fibroblasts cultured in 2-D, with an approximate doubling in the cell circumference with an increase in substrate stiffness from 1600 to 3600 Pa[33]. However, cells encapsulated in a nonporous hydrogel observe the inverse effect as a function of stiffness, likely due to higher resistance to cell-mediated degradation of the hydrogel at higher stiffnesses, which can be controlled by modifying polymer backbone concentration or crosslinking ratio[8,34]. A similar relationship has been observed for transfection as a function of stiffness and dimensionality, suggesting a correlation between cell spreading and transfection[8,9]. Given this, we next sought to evaluate the effect of tuning MAP scaffold stiffness on cell spreading, proliferation, and transfection by increasing the microgel

crosslinking ratio. Gel formulations resulting in a nonporous G' range of 1810 to 3646 Pa—corresponding to overall MAP G' of 222 to 970 Pa (Figure 2G–H)—were tested. The other gel formulation parameters were kept constant at 100–200 μm microgel filter range, RGD concentration of 500 μM, and RGD clustering ratio of 2:1 mmol RGD:mmol HA. Increasing MAP stiffness by increasing the crosslinking ratio significantly enhanced cell spreading, but not cell proliferation (Figure 5A–D). Furthermore, transgene expression increased by 2.28-fold and 2.25-fold by 2 and 6 days after transfection, respectively, when the scaffold stiffness was increased 4.4-fold from 222 to 970 Pa (Figure 5E). As such, spreading and transfection appear to increase with increasing MAP scaffold stiffness, in agreement with results from studies of 2-D culture. However, it is possible that the degree of crosslinking could reduce porosity and RGD presentation to an extent, and this is a point to consider investigating as surface characterizations technologies improve for use with our microgel system. Overall, the results suggest that cell spreading and transfection in MAP scaffolds may be characterized as more similar to that in 2-D than in 3-D. This is also supported by our recent work into the mechanisms and pathways influenced by MAP transfection, with a dependence on microtubule dynamics to the same effect at 2-D cultures, although the internalization and actin signaling cascades did differ[20]. However, the previous study was only done under a single set of MAP physical properties, due to the number of combinations able to be explored, and the results may not translate across all of those explored in this study.

3.4 Effects of MAP cell adhesion properties on transfection

A popular strategy to promote cell attachment to biomaterials is to incorporate integrin-binding peptides such as RGD into the biomaterial formulation. It has been well demonstrated in literature that the concentration and presentation of cell adhesion motifs on a substrate can affect both cell spreading and subsequent gene transfer[7,8,34,35]. With MAP scaffolds, the use of microgels allows for a highly customizable system for ligand presentation across beads and on an individual bead. To understand how tuning cell adhesion characteristics of the MAP hydrogel can affect cell spreading and gene transfer, we manipulated either the concentration or clustering presentation of RGD peptides throughout the gel. Kong et al.[7] found that while increasing RGD concentration increased cell surface area, proliferation, and gene transfer in 2-D, maintaining a constant RGD concentration but with increased peptide clustering resulted in a decrease in proliferation rate and gene transfer without any effect on cell spreading. To first test the effects of overall RGD concentration in MAP scaffolds, the gel was formulated to contain RGD peptides at an overall concentration of 100, 250, 500, or 1000 μM. In all four of these conditions, the formulations were such that there were two RGD peptides conjugated to one HA molecule for the subset of HA molecules containing RGD (Figure 6A). Regardless of RGD concentration, all physical properties were kept constant, including the annealed MAP stiffness and size of microgels at a G' of 222 Pa and sieving range 100–200 μm, respectively. HDFs cultured in MAP gels containing an RGD concentration lower than 500 μM resulted in overall significantly less spreading, lower proliferation, and lower transgene expression than in gel with RGD concentrations of 500 or 1000 μM (Figure 6B–F). These results are consistent with what has previously been reported for the effects of RGD concentration on gene transfer in 2-D[7]. In contrast, it was found that an intermediate concentration of 100 μM RGD resulted in the

highest transfection as compared to 10 and 400 μM for D1 mouse mesenchymal stem cells encapsulated within a 3-D nonporous hydrogel[8], a difference which may be due to the use of a different cell line or the difference in cellular microenvironment between the MAP gel and a nonporous gel. While preliminary in characterization, this may point to the MAP microenvironment giving a similar effect for adhesion as for cells cultured in 2-D on tissue culture plastic. Previous studies have identified that several other mechanisms for transgene expression in MAP also appear to match those in 2-D[20], but more mechanistic studies are needed to fully understand the relation between cell adhesion in MAP and integrin signaling effects on transfection.

To test the effects of RGD clustering, 1, 2, 4, or 12 RGD peptides were conjugated to one HA molecule for the subset of HA molecules containing RGD, while the overall RGD concentration of all four conditions was kept constant at 500 μM (Figure 7A). Again, all other physical properties were kept constant. Interestingly, there was no significant effect on cell spreading and overall viability as a function of RGD clustering, though 2 and 4 mmol RGD:mmol HA did result in higher average cell surface areas (Figure 7B–E). However, transgene expression in the highest clustering ratio of 12 mmol RGD:mmol HA did exhibit the lowest cumulative transgene expression especially by 6 days (Figure 7F). Kong et al.[7] did also report lower transgene expression at the highest clustering ratio tested and suggested that this may be due to the relatively large spacing between RGD ligand clusters adversely affecting integrin signaling and therefore overall growth rate. It could be worth investigating if the effects observed for varied RGD concentrations and stiffness are consistent at other annealed MAP stiffnesses, since both stiffness and RGD regulate cell spreading and proliferation to an extent. While inclusion of RGD at different concentrations does not exhaust the availability of free norbornenes on the gel backbone even after crosslinking, resulting in a consistent stiffness regardless of RGD patterning, a range of stiffnesses could be tailored for the each layout to improve viability. This would require more extensive studies outside of our intended scope but are good considerations for future optimization of the MAP scaffold.

3.5 Effect of integrin specificity on transfection

We next studied the role of integrin binding in guiding gene transfer. Previous studies have demonstrated that specific or preferential integrin activation has differential effects on stem cell differentiation[36], epithelial cell phenotype[37], and vessel regeneration[38], demonstrating the importance of integrin specificity in cellular processes. This suggests that the current near-ubiquitous strategy of incorporating RGD ligands into biomaterials may not be optimal for promoting specific cellular processes, given the primary ability of RGD to bind to αv integrins[37]. Furthermore, presenting short integrin-binding peptides in biomaterials result in significantly reduced cell adhesion affinity when compared to identical molar concentrations of the same peptide included in its endogenous three-dimensional full-length protein structure[38]. Here, we sought to study the effects of integrin specificity on HDF spreading, proliferation, and gene transfer. To our knowledge, this is the first investigation of the role of specificity of integrin activation in modulating gene transfer.

One method of determining integrin specificity is to control the conformational stability of the RGD-containing ninth and tenth domains of fibronectin (Fn III9–10) by introducing either a Leu-Pro point mutation at position 1408 (9*10) or a labile 4 x Gly linker (9(4G)10) between the two domains; these variants have been demonstrated to preferentially bind to α3/α5β1 or αvβ3 integrins, respectively[36,38]. In place of RGD, these recombinant fibronectin fragments were covalently tethered to the HA-Norb backbone at a final concentration of 5 μM and used to form microgels. This concentration was chosen in light of previous studies which demonstrated spreading with fibronectin fragment concentrations of that magnitude, levels comparable to spreading observed in environments with RGD concentrations on the order of 10^2 μM[37,39]. The annealed MAP stiffness and size of microgels were also kept constant at a G' of 222 Pa and sieving range 100–200 μm, respectively. HDFs cultured in MAP gels which preferentially activate α3/α5β1 integrins exhibited lower average cell surface area than in MAP gels which preferentially activate αvβ3 integrins (Figure 8A–C). However, α3/α5β1-activating gels interestingly resulted in higher overall proliferation and, notably, higher transgene expression after transfection despite less spreading (Figure 8D–E).

In investigating effects of both physical and cell-adhesive properties of MAP scaffolds on cell behavior, we noticed that the extent of cell spreading appeared to correlate with cell proliferation and that both properties appeared to correlate with transgene expression in studies of microgel size, stiffness, and RGD concentration. The trends were maintained even after normalizing expression to proliferation levels at time of transfection at day 2 (Supplementary Figure 2). This is consistent with previous 2-D studies of preosteoblasts and mesenchymal stem cells which found similar trends[7,9,40]. However, we speculate that proliferation more heavily influences gene transfer and transgene expression, given our finding that α3/α5β1-activating gels increased overall proliferation and transgene expression despite a decrease in spreading. This suggests that integrin-dependent differences in gene transfer may in fact be independent of the extent of cell spreading, with a stronger correlation to proliferation (Figure 8). The dependence of polyplex-mediated gene transfer on cell cycle has previously been reported in 2-D[41]. Transgene expression was 10x-50x higher when polyplex-mediated transfection occurred during S, G2, or M phases of cell division, perhaps due to nuclear membrane degradation during phases closer to the mitotic M phase. This suggests that if certain substrate characteristics can trigger increased cell proliferation, this can directly affect the ability of seeded cells to be efficiently transfected and subsequently significantly increase downstream transgene expression.

4 Conclusion

In this study, we performed *in vitro* studies to examine how MAP hydrogel properties can be tuned to enhance non-viral gene transfer from polyplexes. Microgel diameters of 60–200 μm, increased microgel stiffness, RGD concentrations of at least 500 μM, and an RGD clustering ratio of less than 12 mmol RGD:mmol HA resulted in the highest transgene expression. These modifications initially appeared to correlate both with cell spreading and cell proliferation. However, MAP gels which preferentially activated β_1 integrins resulted in enhanced proliferation and transgene expression but decreased average cell spreading, decoupling the trend of proliferation from spreading and suggesting that transgene

expression may be independent of cell spreading. Overall, these findings demonstrate that MAP scaffolds can serve as a highly tunable platform for studying polyplex-mediated gene transfer in a homogeneously seeded, uniformly transfected 3-D culture environment. These findings will also inform future design criteria when integrating non-viral gene delivery with therapeutically relevant MAP scaffolds for tissue repair *in vivo*.

Supplementary Material

Refer to Web version on PubMed Central for supplementary material.

5 Acknowledgements

We thank Talar Tokatlian for proofreading assistance and Shruti Sharma for technical assistance. We would like to acknowledge the support of funding from NIH (R01HL110592 and T32GM067555).

6 References

[1]. Yin H, Kanasty RL, Eltoukhy AA, Vegas AJ, Robert Dorkin J, Anderson DG, Non-viral vectors for gene-based therapy, (2014). doi:10.1038/nrg3763.

[2]. Jafari M, Soltani M, Naahidi S, Karunaratne DN, Chen P, Nonviral Approach for Targeted Nucleic Acid Delivery, Curr. Med. Chem. 19 (2012) 197–208. doi:10.2174/092986712803414141. [PubMed: 22320298]

[3]. Hardee CL, Arévalo-Soliz LM, Hornstein BD, Zechiedrich L, Advances in non-viral DNA vectors for gene therapy, Genes (Basel). 8 (2017) 65. doi:10.3390/genes8020065.

[4]. Kasputis T, Pannier AK, The role of surface chemistry-induced cell characteristics on nonviral gene delivery to mouse fibroblasts., J. Biol. Eng. 6 (2012) 17. doi:10.1186/1754-1611-6-17. [PubMed: 22967455]

[5]. Bengali Z, Rea JC, Shea LD, Gene expression and internalization following vector adsorption to immobilized proteins: Dependence on protein identity and density, J. Gene Med. 9 (2007) 668–678. doi:10.1002/jgm.1058. [PubMed: 17533618]

[6]. Dhaliwal A, Maldonado M, Han Z, Segura T, Differential uptake of DNApoly(ethylenimine) polyplexes in cells cultured on collagen and fibronectin surfaces., Acta Biomater. 6 (2010) 3436–47. doi:10.1016/j.actbio.2010.03.038. [PubMed: 20371304]

[7]. Kong HJ, Hsiong S, Mooney DJ, Nanoscale cell adhesion ligand presentation regulates nonviral gene delivery and expression., Nano Lett. 7 (2007) 161–6. doi:10.1021/nl062485g. [PubMed: 17212457]

[8]. Gojgini S, Tokatlian T, Segura T, Utilizing cell-matrix interactions to modulate gene transfer to stem cells inside hyaluronic acid hydrogels., Mol. Pharm. 8 (2011) 1582–91. doi:10.1021/mp200171d. [PubMed: 21823632]

[9]. Kong HJ, Liu J, Riddle K, Matsumoto T, Leach K, Mooney DJ, Non-viral gene delivery regulated by stiffness of cell adhesion substrates., Nat. Mater. 4 (2005) 460–4. doi:10.1038/nmat1392. [PubMed: 15895097]

[10]. Teo BKK, Goh SH, Kustandi TS, Loh WW, Low HY, Yim EKF, The effect of micro and nanotopography on endocytosis in drug and gene delivery systems, Biomaterials. 32 (2011) 9866–9875. doi:10.1016/j.biomaterials.2011.08.088. [PubMed: 21924770]

[11]. Tibbitt MW, Anseth KS, Hydrogels as extracellular matrix mimics for 3D cell culture, Biotechnol. Bioeng. 103 (2009) 655–663. doi:10.1002/bit.22361. [PubMed: 19472329]

[12]. Liang X, Boppart SA, Biomechanical properties of in vivo human skin from dynamic optical coherence elastography., IEEE Trans. Biomed. Eng. 57 (2010) 953–9. doi:10.1109/TBME.2009.2033464. [PubMed: 19822464]

[13]. Budday S, Nay R, de Rooij R, Steinmann P, Wyrobek T, Ovaert TC, Kuhl E, Mechanical properties of gray and white matter brain tissue by indentation., J. Mech. Behav. Biomed. Mater. 46 (2015) 318–30. doi:10.1016/j.jmbbm.2015.02.024. [PubMed: 25819199]

[14]. Griffin M, Premakumar Y, Seifalian A, Butler PE, Szarko M, Biomechanical Characterization of Human Soft Tissues Using Indentation and Tensile Testing., J. Vis. Exp. (2016). doi:10.3791/54872.

[15]. Griffin DR, Weaver WM, Scumpia PO, Di Carlo D, Segura T, Accelerated wound healing by injectable microporous gel scaffolds assembled from annealed building blocks, Nat. Mater. 14 (2015) 737–744. doi:10.1038/nmat4294.Accelerated. [PubMed: 26030305]

[16]. Sideris E, Griffin DR, Ding Y, Li S, Weaver WM, Di Carlo D, Hsiai T, Segura T, Particle Hydrogels Based on Hyaluronic Acid Building Blocks, ACS Biomater. Sci. Eng. 2 (2016) 2034–2041. doi:10.1021/acsbiomaterials.6b00444.

[17]. Nih LR, Sideris E, Carmichael ST, Segura T, Injection of Microporous Annealing Particle (MAP) Hydrogels in the Stroke Cavity Reduces Gliosis and Inflammation and Promotes NPC Migration to the Lesion, Adv. Mater. 29 (2017) 1606471. doi:10.1002/adma.201606471.

[18]. Mehrabian A, Abousleiman YN, Mapstone TB, El-Amm CA, Dual-porosity poroviscoelasticity and quantitative hydromechanical characterization of the brain tissue with experimental hydrocephalus data, J. Theor. Biol. 384 (2015) 19–32. doi:10.1016/J.JTBI.2015.08.001. [PubMed: 26277735]

[19]. Wagner A, Ehlers W, A Porous Media Model to Describe the Behaviour of Brain Tissue, PAMM · Proc. Appl. Math. Mech. 8 (2008) 10201–10202. doi:10.1002/pamm.200810201.

[20]. Truong NF, Lesher-Pérez SC, Kurt E, Segura T, Pathways Governing Polyethylenimine Polyplex Transfection in Microporous Annealed Particle Scaffolds, Bioconjug. Chem. (2018) acs.bioconjchem.8b00696. doi:10.1021/acs.bioconjchem.8b00696.

[21]. Desmond KW, Weeks ER, Influence of particle size distribution on random close packing of spheres, Phys. Rev. E - Stat. Nonlinear, Soft Matter Phys. 90 (2014) 1–6. doi:10.1103/PhysRevE.90.022204.

[22]. Nawaz S, Sánchez P, Bodensiek K, Li S, Simons M, Schaap IAT, Cell ViscoElasticity Measured with AFM and Optical Trapping at Sub-Micrometer Deformations, PLoS One. 7 (2012) e45297. doi:10.1371/journal.pone.0045297. [PubMed: 23028915]

[23]. Lulevich Valentin, Zink Tiffany, Chen Huan-Yuan, § and Liu Fu-Tong, Liu Gang-yu, Cell Mechanics Using Atomic Force Microscopy-Based Single-Cell Compression, (2006). doi:10.1021/LA060561P.

[24]. Alge DL, Azagarsamy MA, Donohue DF, Anseth KS, Synthetically Tractable Click Hydrogels for Three-Dimensional Cell Culture Formed Using Tetrazine–Norbornene Chemistry, Biomacromolecules. 14 (2013) 949–953. doi:10.1021/bm4000508. [PubMed: 23448682]

[25]. Hansell CF, Espeel P, Stamenović MM, Barker IA, Dove AP, Du Prez FE, O'Reilly RK, Additive-Free Clicking for Polymer Functionalization and Coupling by Tetrazine–Norbornene Chemistry, J. Am. Chem. Soc. 133 (2011) 13828–13831. doi:10.1021/ja203957h. [PubMed: 21819063]

[26]. Zeltinger J, Sherwood JK, Graham DA, Müeller R, Griffith LG, Effect of Pore Size and Void Fraction on Cellular Adhesion, Proliferation, and Matrix Deposition, Tissue Eng. 7 (2001) 557–572. doi:10.1089/107632701753213183. [PubMed: 11694190]

[27]. Loh QL, Choong C, Three-Dimensional Scaffolds for Tissue Engineering Applications: Role of Porosity and Pore Size, Tissue Eng. Part B Rev. 19 (2013) 485–502. doi:10.1089/ten.teb.2012.0437. [PubMed: 23672709]

[28]. Murphy CM, Haugh MG, O'Brien FJ, The effect of mean pore size on cell attachment, proliferation and migration in collagen-glycosaminoglycan scaffolds for bone tissue engineering, Biomaterials. 31 (2010) 461–466. doi:10.1016/j.biomaterials.2009.09.063. [PubMed: 19819008]

[29]. Mandal BB, Kundu SC, Cell proliferation and migration in silk fibroin 3D scaffolds, Biomaterials. 30 (2009) 2956–2965. doi:10.1016/j.biomaterials.2009.02.006. [PubMed: 19249094]

[30]. Matsiko A, Gleeson JP, O'Brien FJ, Scaffold Mean Pore Size Influences Mesenchymal Stem Cell Chondrogenic Differentiation and Matrix Deposition, Tissue Eng. Part A. 21 (2015) 486–497. doi:10.1089/ten.tea.2013.0545. [PubMed: 25203687]

[31]. Hu B, Leow WR, Amini S, Nai B, Zhang X, Liu Z, Cai P, Li Z, Wu Y-L, Miserez A, Lim CT, Chen X, Orientational Coupling Locally Orchestrates a Cell Migration Pattern for Re-Epithelialization, Adv. Mater. 29 (2017) 1700145. doi:10.1002/adma.201700145.

[32]. Hopp I, Michelmore A, Smith LE, Robinson DE, Bachhuka A, Mierczynska A, Vasilev K, The influence of substrate stiffness gradients on primary human dermal fibroblasts, Biomaterials. 34 (2013) 5070–5077. doi:10.1016/j.biomaterials.2013.03.075. [PubMed: 23587444]

[33]. Yeung T, Georges PC, Flanagan LA, Marg B, Ortiz M, Funaki M, Zahir N, Ming W, Weaver V, Janmey PA, Effects of substrate stiffness on cell morphology, cytoskeletal structure, and adhesion, Cell Motil. Cytoskeleton. 60 (2005) 24–34. doi:10.1002/cm.20041. [PubMed: 15573414]

[34]. Lei Y, Gojgini S, Lam J, Segura T, The spreading, migration and proliferation of mouse mesenchymal stem cells cultured inside hyaluronic acid hydrogels., Biomaterials. 32 (2011) 39–47. doi:10.1016/j.biomaterials.2010.08.103. [PubMed: 20933268]

[35]. Lam J, Segura T, The modulation of MSC integrin expression by RGD presentation, Biomaterials. 34 (2013) 3938–3947. doi:10.1016/j.biomaterials.2013.01.091. [PubMed: 23465825]

[36]. Martino MM, Mochizuki M, Rothenfluh DA, Rempel SA, Hubbell JA, Barker TH, Controlling integrin specificity and stem cell differentiation in 2D and 3D environments through regulation of fibronectin domain stability, Biomaterials. 30 (2009) 1089–1097. doi:10.1016/j.biomaterials.2008.10.047. [PubMed: 19027948]

[37]. Brown AC, Rowe JA, Barker TH, Guiding Epithelial Cell Phenotypes with Engineered Integrin-Specific Recombinant Fibronectin Fragments, Tissue Eng. Part A. 17 (2011) 139–150. doi:10.1089/ten.tea.2010.0199. [PubMed: 20695776]

[38]. Li S, Nih LR, Bachman H, Fei P, Li Y, Nam E, Dimatteo R, Carmichael ST, Barker TH, Segura T, Hydrogels with precisely controlled integrin activation dictate vascular patterning and permeability, Nat. Mater. 16 (2017). doi:10.1038/nmat4954.

[39]. Lam J, Truong NF, Segura T, Design of cell-matrix interactions in hyaluronic acid hydrogel scaffolds., Acta Biomater. 10 (2014) 1571–1580. doi:10.1016/j.actbio.2013.07.025. [PubMed: 23899481]

[40]. Dhaliwal A, Lam J, Maldonado M, Lin C, Segura T, Extracellular matrix modulates non-viral gene transfer to mouse mesenchymal stem cells, Soft Matter. 8 (2012) 1451–1459. doi:10.1039/C1SM06591B.

[41]. Brunner S, Sauer T, Carotta S, Cotten M, Saltik M, Wagner E, Cell cycle dependence of gene transfer by lipoplex, polyplex and recombinant adenovirus., Gene Ther. 7 (2000) 401–7. doi:10.1038/sj.gt.3301102. [PubMed: 10694822]

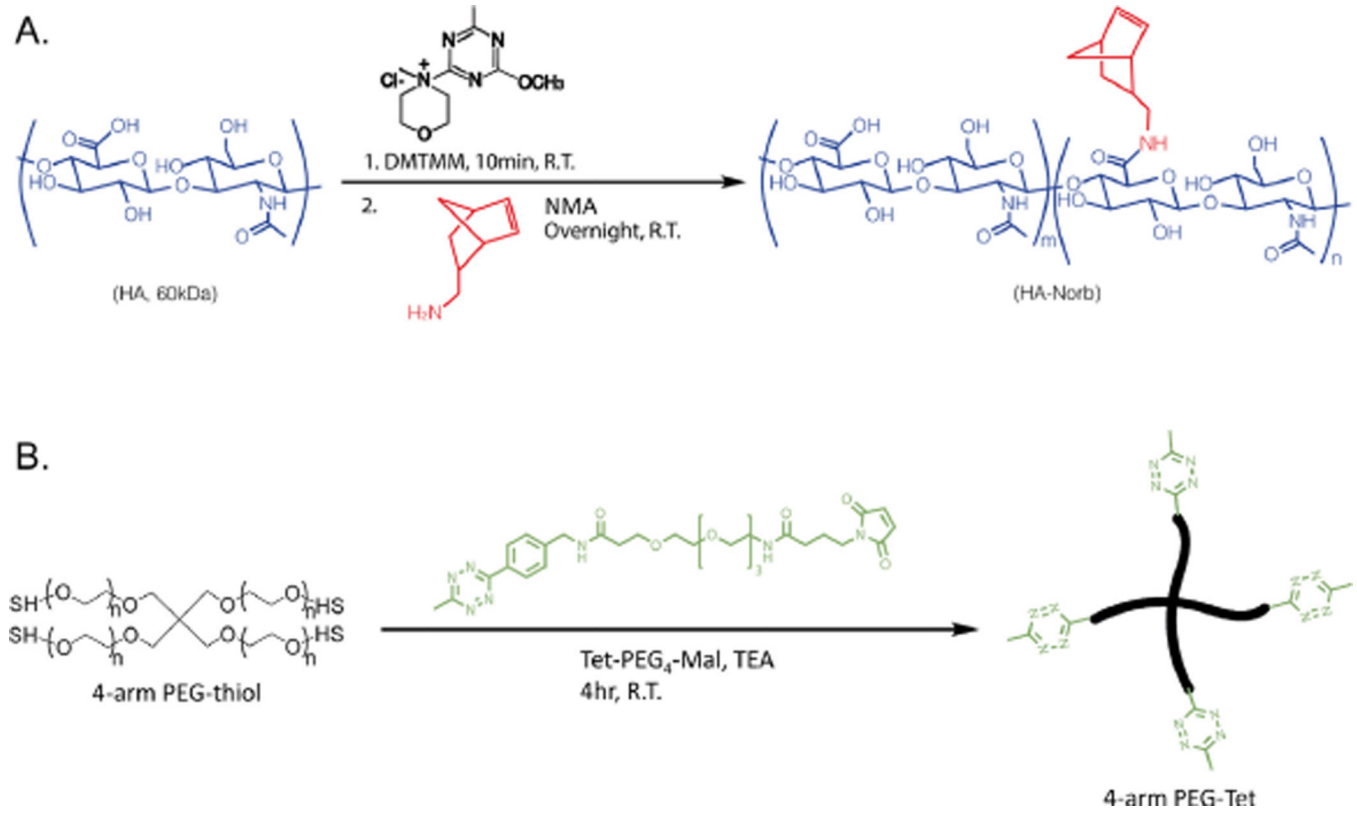

Fig. 1.

Overview of HA-Norb and PEG-Tet synthesis. A) 2-step reaction for HA-Norb synthesis from hyaluronic acid and NMA. The the carboxylic acids on the HA polymer were activated using DMTMM, followed by overnight reaction with NMA to add the norbornene groups. B) Thiol-ene reaction for PEG-Tet synthesis from 4-arm PEG-thiol and Tet-PEG-Mal.

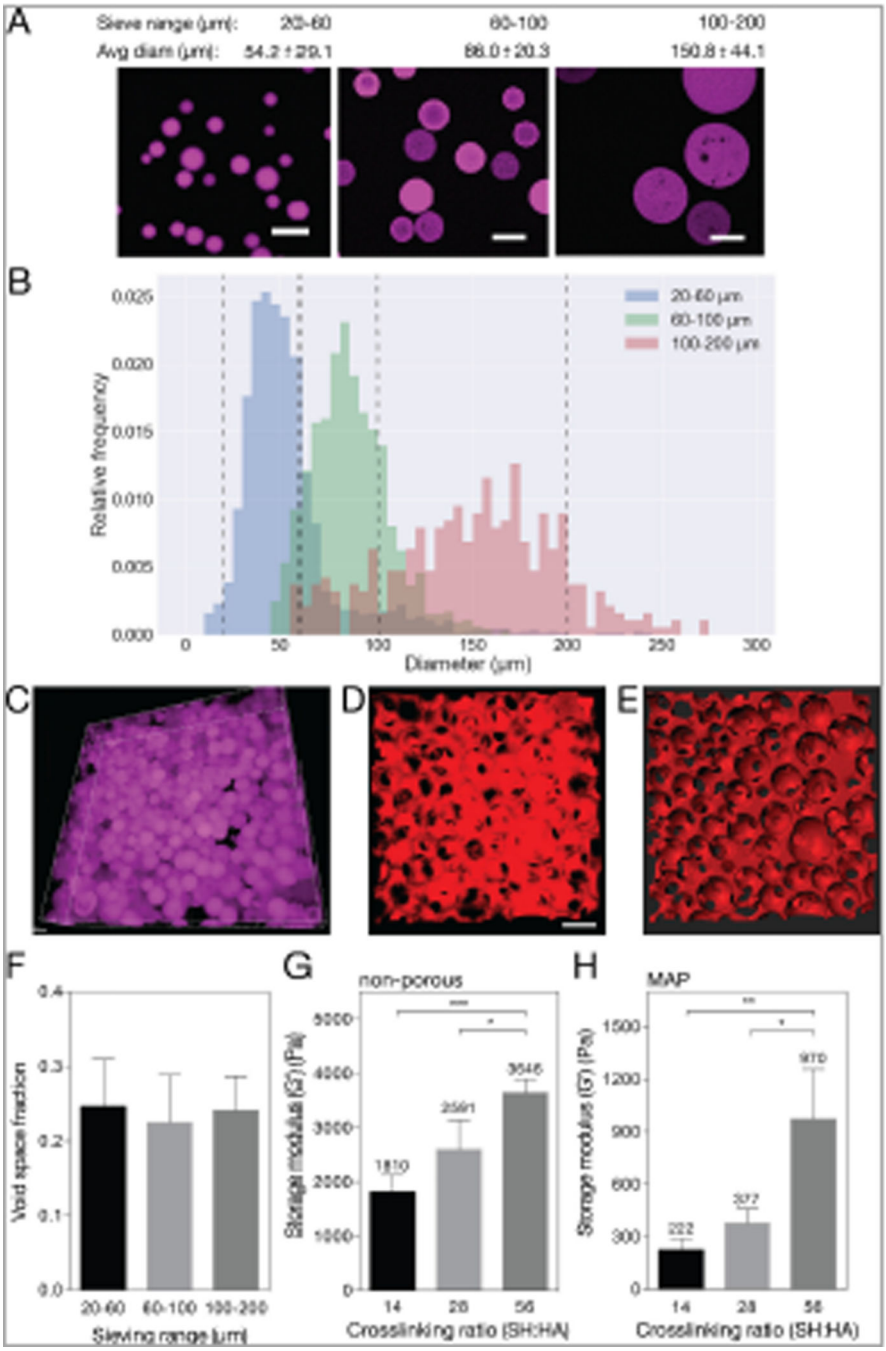

Fig. 2.

Characterization of MAP gel properties. A) Confocal microscopy images of Alexa Fluor 647-tagged HA microgels after swelling and sieving to collect gel between the 20–60 lm filters, between the 60–100 lm filters, and between the 100–200 lm filters. Scale bar = 100 lm. B) Relative frequency histogram of size distributions of gel collected between the different sieving ranges. Dashed lines indicate filter pore size. C) Z-stack of annealed MAP gel using gel collected between the 60–100 lm filters. D) Visualization of void space within the MAP scaffold by using high-molecular-weight TRITC-dextran to fill pores of MAP gel.

Scale bar = 200 lm. E) IMARIS rendering of void space volume from z-stack in Fig. 1D. Scale bar = 200 lm. F) Void space fraction of annealed MAP gel consisting of the different sieving ranges as calculated from IMARIS renderings of void space volume, for a constant crosslinking ratio of 14. Storage moduli of G) nonporous HA-Norb gels and H) annealed MAP gel with microgels crosslinked at different crosslinking ratios as measured by oscillation rheometry with average storage moduli noted above each condition. (*$p < 0.05$, **$p < 0.01$, and ***$p < 0.001$).

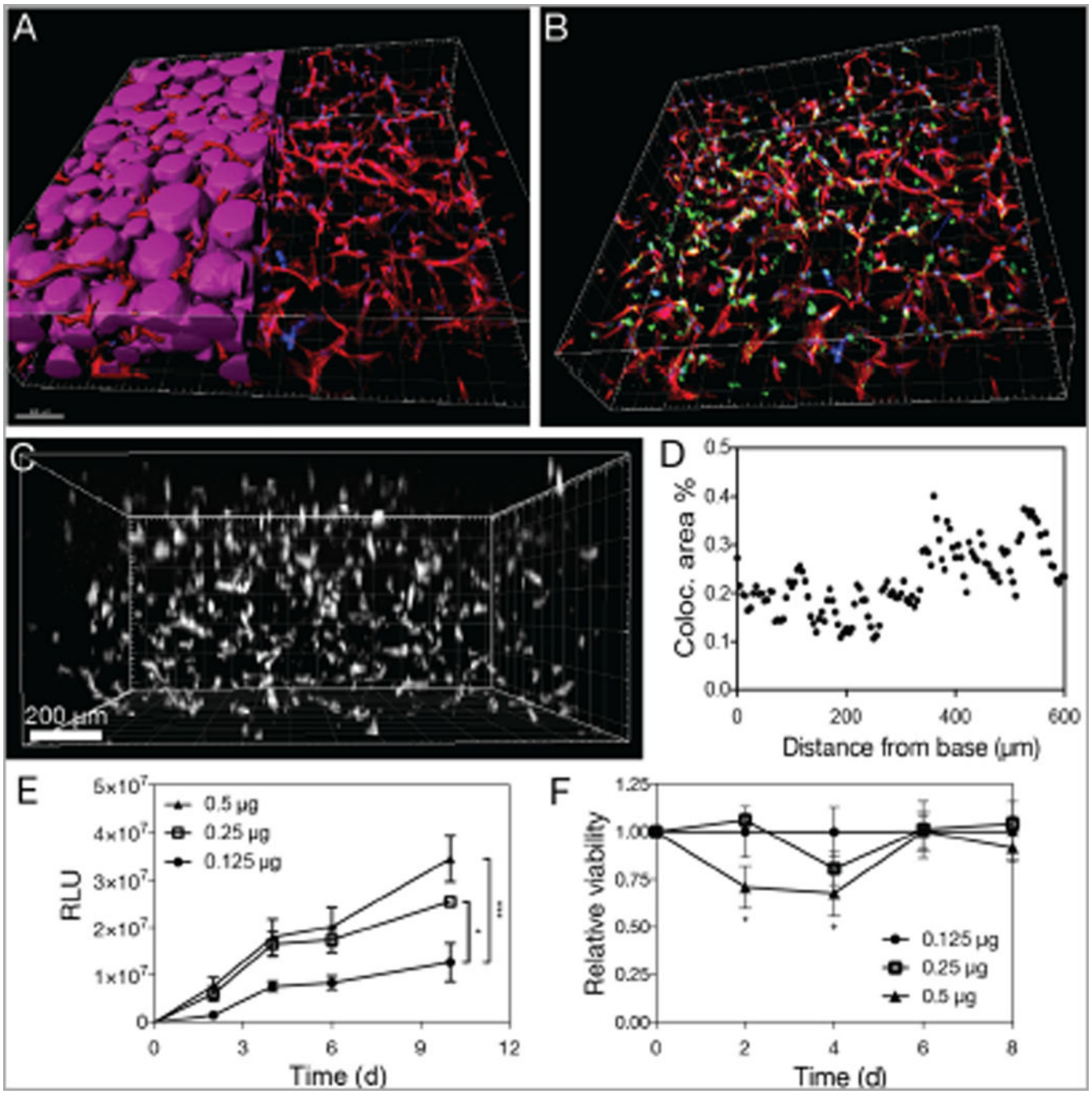

Fig. 3.

Characterization of HDF culture and polyplex distribution, transgene expression, and cell viability following transfection in MAP gels. A) 3-D rendering of z-stack of HDFs (actin in red, nuclei in blue) cultured in MAP gels 2 days after seeding. IMARIS was used to generate a volume render of the MAP gel of the left half of the image. Scale bar = 150 lm. B) 3-D render of HDFs cultured in MAP gels (MAP gel not shown) with YOYO-1-labelled polyplexes (green) after 4 h of polyplex exposure. Scale bar = 200 lm. C). 3-D render of co-localization of YOYO-1 polyplexes and cell actin after 4-hour transfection in MAP gel.

Vertical axis represents the z-axis. D) Quantification of area of polyplex and actin co-localization along z-axis. E) Transgene expression of HDF culture in MAP gels over time as a function of DNA polyplex dose (*$p < 0.05$ and ***$p < 0.001$). F) Relative cell viability over time as measured using the PrestoBlue assay as a function of DNA polyplex dose (*$p < 0.05$ between 0.5 lg and other two conditions; +$p < 0.05$ between 0.5 lg and 0.125 lg). (For interpretation of the references to colour in this figure legend, the reader is referred to the web version of this article.)

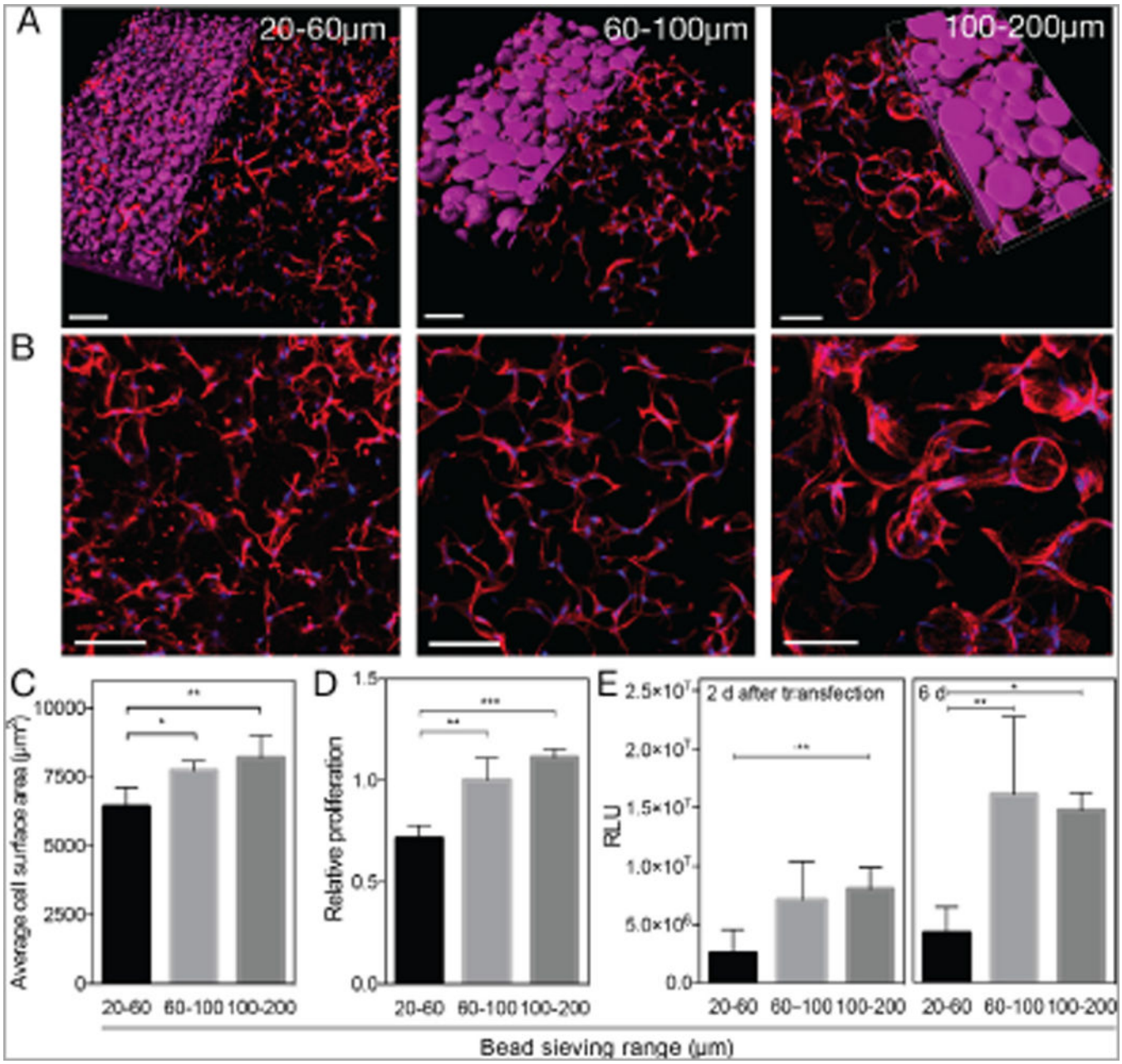

Fig. 4.

Effect of microgel diameter on HDF spreading and transfection in MAP gels. A) 3-D renders and B) aerial views of HDF spreading (actin in red, nuclei in blue) in MAP gels of different microgel sizes after 2 days of culture. Scale bar = 150 lm. C) Quantification of average cell surface area in each size condition using IMARIS. D) Relative cell activity/ proliferation 2 days after seeding using PrestoBlue assay. E) Cumulative transgene expression 2 and 6 days after transfection. (*$p < 0.05$, **$p < 0.01$, and ***$p < 0.001$).(For interpretation of the references to colour in this figure legend, the reader is referred to the web version of this article.)

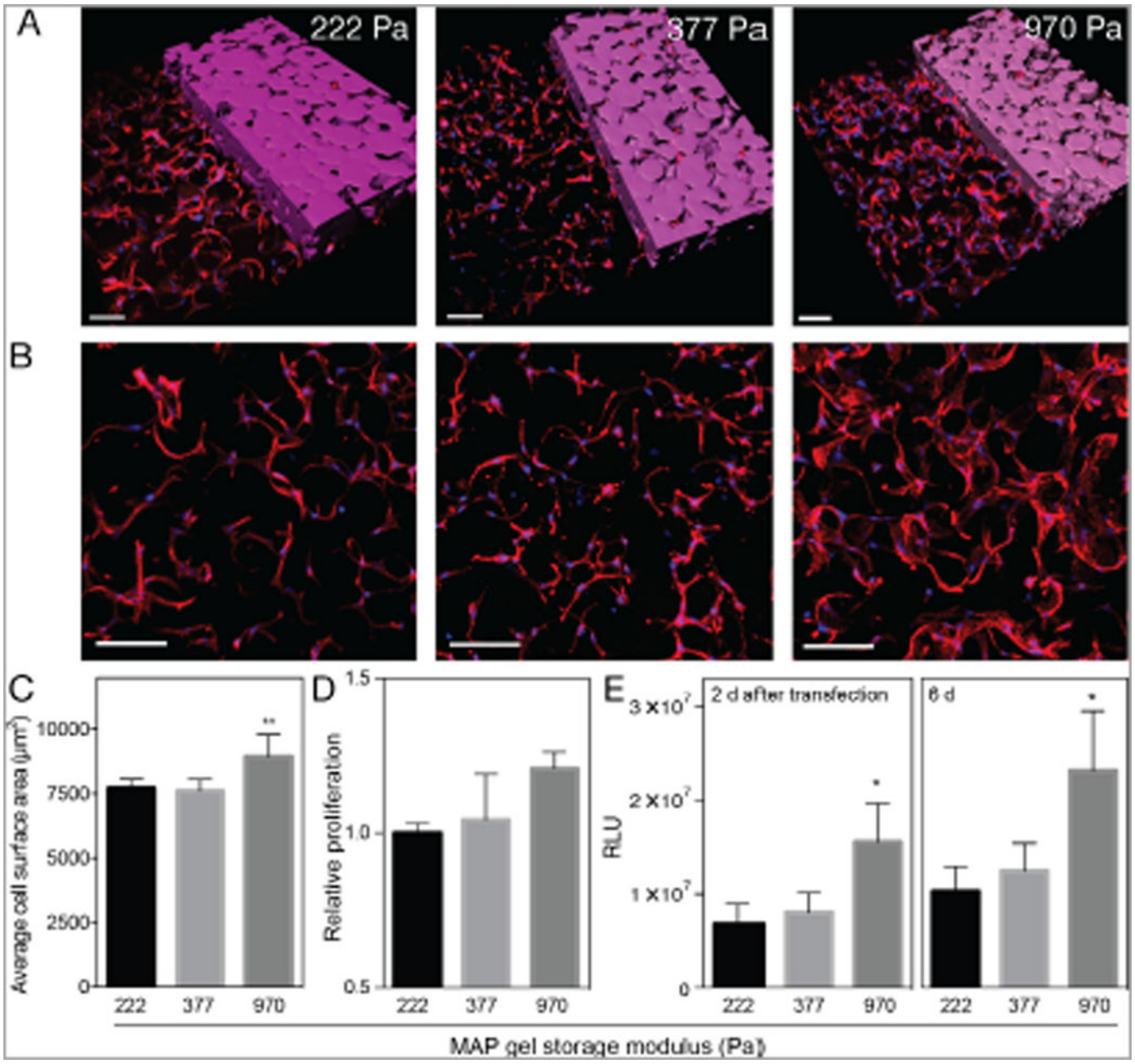

Fig. 5.

Effect of MAP gel stiffness on HDF spreading and transfection in MAP gels. A) 3-D renders and B) aerial views of HDF spreading (actin in red, nuclei in blue) in MAP gels of different storage moduli after 2 days of culture. Scale bar = 150 lm. C) Quantification of average cell surface area in each stiffness condition using IMARIS. D) Relative cell activity/proliferation 2 days after seeding using PrestoBlue assay. E) Cumulative transgene expression 2 and 6 days after transfection. (*$p < 0.05$, **$p < 0.01$, and ***$p < 0.001$).(For interpretation of the references to colour in this figure legend, the reader is referred to the web version of this article.)

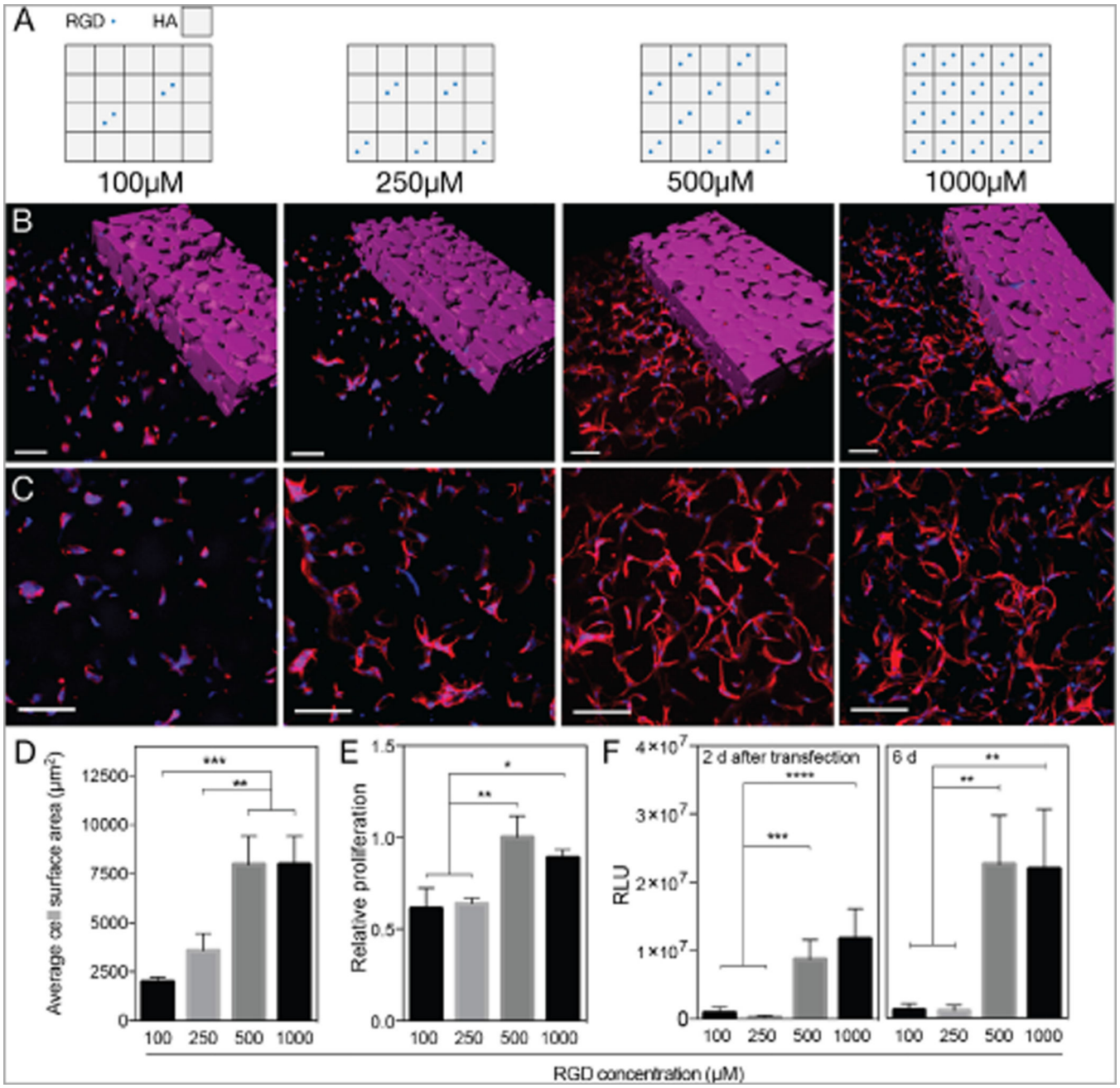

Fig. 6.

Effect of RGD concentration on HDF spreading and transfection in MAP gels. A) Schematic of RGD presentation in conditions of varying RGD concentrations. B) 3-D renders and C) aerial views of HDF spreading (actin in red, nuclei in blue) in MAP gels of different RGD concentrations after 2 days of culture. Scale bar = 150 lm. D) Quantification of average cell surface area in each RGD concentration condition using IMARIS. E) Relative cell activity/ proliferation 2 days after seeding using PrestoBlue assay. F) Cumulative transgene expression 2 and 6 days after transfection. (*p < 0.05, **p < 0.01, and ***p < 0.001). (For

interpretation of the references to colour in this figure legend, the reader is referred to the web version of this article.)

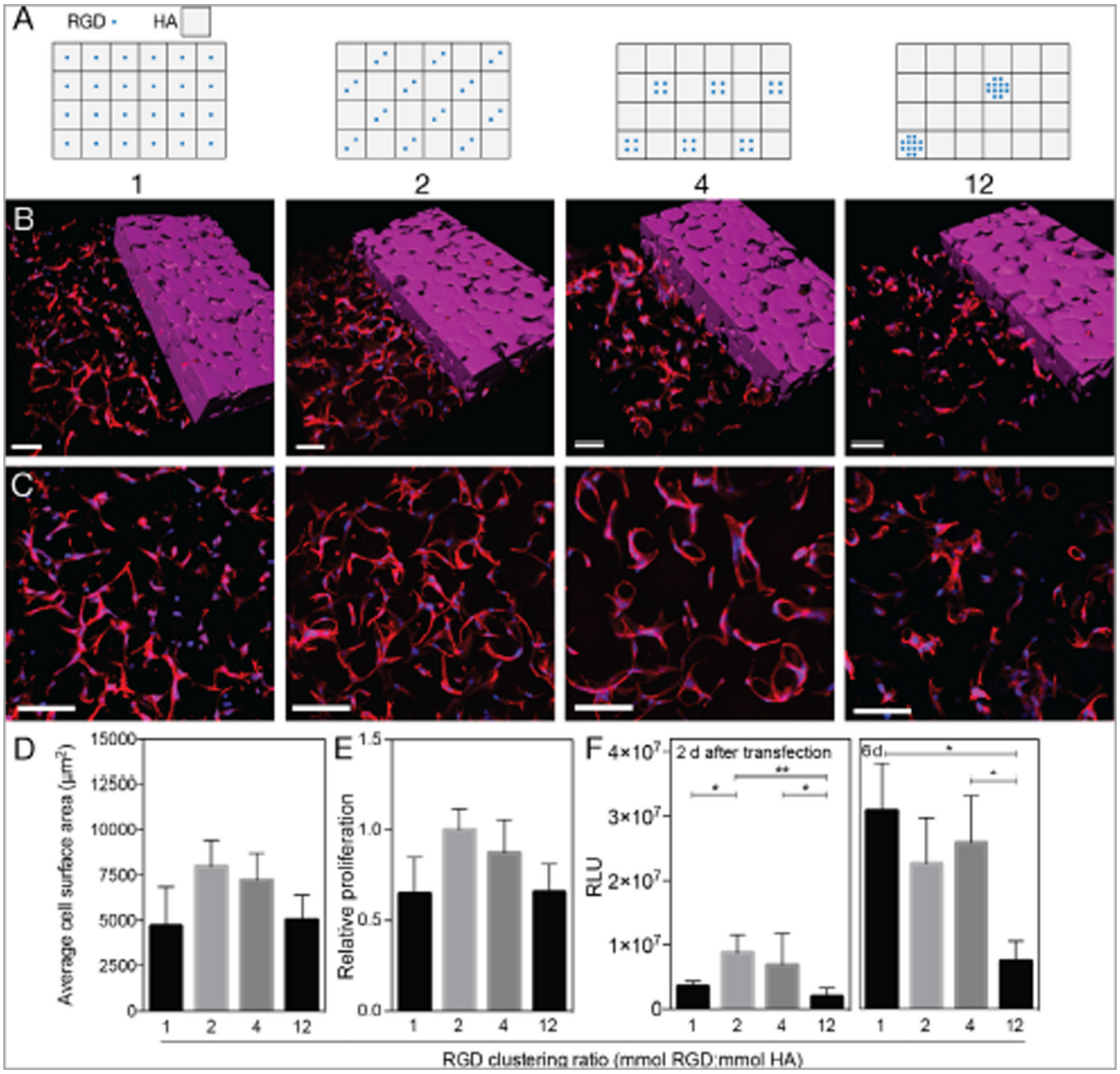

Fig. 7.

Effect of RGD clustering ratio (mmol RGD/mmol HA) on HDF spreading and transfection in MAP gels. A) Schematic of RGD presentation in conditions of varying RGD clustering ratios. B) 3-D renders and C) aerial views of HDF spreading (actin in red, nuclei in blue) in MAP gels of different RGD clustering ratios after 2 days of culture. Scale bar = 150 lm. D) Quantification of average cell surface area in each RGD clustering condition using IMARIS. E) Relative cell activity/proliferation 2 days after seeding using PrestoBlue assay. F) Cumulative transgene expression 2 and 6 days after transfection. (*$p < 0.05$, **$p < 0.01$, and ***$p < 0.001$). (For interpretation of the references to colour in this figure legend, the reader is referred to the web version of this article.)

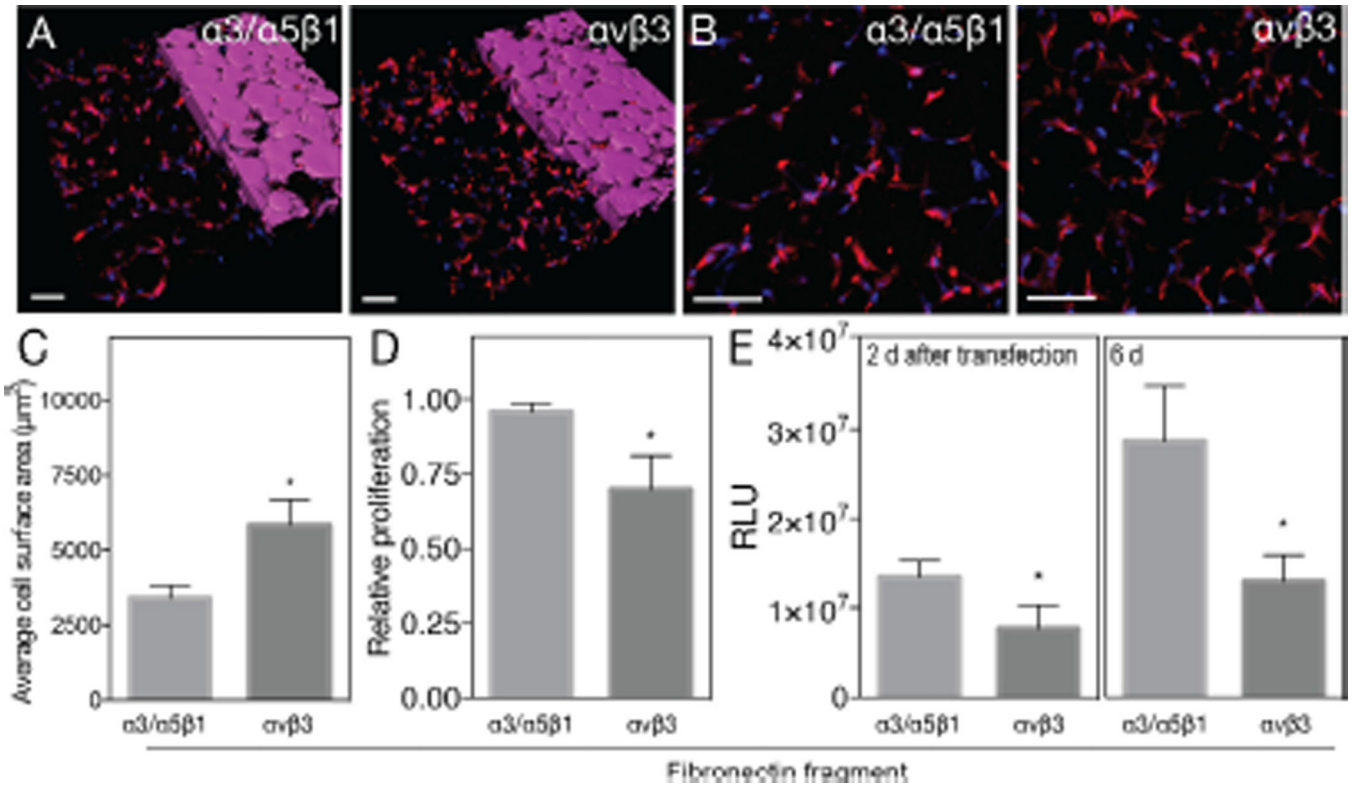

Fig. 8.

Effect of integrin specificity as controlled by cell adhesion ligand on HDF spreading and transfection in MAP gels. A) 3-D renders and B) aerial views of HDF spreading (actin in red, nuclei in blue) in MAP gels of different cell adhesion ligand (fibronectin fragment 9*10 or fibronectin fragment 9(4G)10 after 2 days of culture. Scale bar = 150 lm. C) Quantification of average cell surface area in each integrin ligand condition using IMARIS. D) Relative cell activity/proliferation 2 days after seeding using PrestoBlue assay. E) Cumulative transgene expression 2 and 6 days after transfection. (*$p < 0.05$, **$p < 0.01$, and ***$p < 0.001$). (For interpretation of the references to colour in this figure legend, the reader is referred to the web version of this article.)